

Tailoring plasmons with metallic nanorod arraysC. Tserkezis,¹ N. Papanikolaou,² E. Almpanis,² and N. Stefanou¹¹*Section of Solid State Physics, University of Athens, Panepistimioupolis, GR-157 84 Athens, Greece*²*Institute of Microelectronics, NCSR "Demokritos," GR-153 10 Athens, Greece*

(Received 1 July 2009; revised manuscript received 31 August 2009; published 24 September 2009)

We report a thorough theoretical study of the optical response of two- and three-dimensional periodic assemblies of metallic nanorods by means of full-electrodynamics calculations using the extended layer-multiple-scattering method. We show that these systems support various types of resonant- and bound-collective plasmon modes, which are tunable over a broad spectral range, and provide a consistent interpretation of the underlying physics. In particular, we reveal the existence of slab plasmon modes with zero group velocity, which can cause evanescent-wave enhancement and enable subwavelength imaging. We discuss extinction spectra of single-layer and multilayer slabs of nanorods in conjunction with relevant complex band-structure diagrams and present a rigorous analysis of the results using group theory. Moreover, we explain some peculiar spectral features which are due to the existence of surface resonances. These can modify the optical response of the system in a controllable manner by using a supporting substrate.

DOI: [10.1103/PhysRevB.80.125124](https://doi.org/10.1103/PhysRevB.80.125124)

PACS number(s): 42.70.Qs, 42.25.Bs, 73.20.Mf, 78.67.Bf

I. INTRODUCTION

Metallic nanostructures exhibit a rich variety of intriguing optical properties due to the interaction of the electromagnetic (EM) field with the free electrons of the metal. Such an excitation can occur at a metal-dielectric interface and is called surface-plasmon polariton or at a metallic nanoparticle and in this case it is termed as particle-plasmon polariton. The distinction accounts for the degree of localization of the plasmon. One of the most attractive features of plasmon excitation is that it is accompanied with local field enhancement and subwavelength focusing. There are several recent reviews on the physics and applications of surface plasmons.¹

Metallic nanoparticles were used since ancient times to color glass. Nowadays, isolated metallic nanoparticles are usually chemically synthesized as colloidal suspensions and come in a variety of shapes and sizes. In the simple case of noble-metal nanospheres, the extinction spectrum is dominated by strong dipole plasmon resonances at visible frequencies. For elongated particles, the threefold degeneracy of these modes is lifted and one obtains a predominant non-degenerate longitudinal mode at lower frequencies as well as doubly degenerate transverse and other modes of mixed character at higher frequencies. These plasmon resonances can be tuned within a relatively broad range from infrared to visible frequencies by a proper choice of the geometrical characteristics, dielectric environment, and material.²⁻¹² Therefore, elongated metallic nanoparticles, such as ellipsoids or cylinders, can be used as efficient and tunable optical antennas for manipulating light at the nanoscale. On the other hand, in metallic nanoparticle aggregates, interacting plasmons provide further possibilities to engineer the spectral response and tailor the light-matter interaction. The concept of plasmon hybridization¹³ has been successfully used to understand the optical properties of metallic nanoparticle pairs^{14,15} as well as the spectra of clusters of such nanoparticles. The physics of this mechanism has much in common with the hybridization of electron states of atoms that form

molecular orbitals; this is why terms such as photonic or plasmonic (meta)molecules are often used in the literature.¹⁶

Recent advances in nanofabrication and nanopatterning open new perspectives to enhance Raman and fluorescence spectroscopic sensitivity,¹⁷⁻²⁰ taking advantage of localized and extended plasmons. Also, plasmon resonances can be made rather sensitive to the dielectric environment and thus they are considered for accurate dielectric-constant monitoring of chemical and biological samples.^{21,22} Concerning possible technological applications, various plasmonic waveguide architectures have been proposed,²³⁻²⁷ and there is a hope that metallic components could be the basic elements of nanophotonic integrated optical circuits. Moreover, light focusing and EM field enhancement due to plasmons may have applications in solar cells,²⁸ in nonlinear optics, and in the development of novel optoelectronic devices.¹

Periodicity is a valuable tool in plasmon engineering. Among the different periodic architectures, regular arrays of metallic nanorods aligned perpendicular to a substrate attract considerable interest, because they offer the possibility to combine plasmon tunability of the individual nanorods with controllable interparticle interaction. In addition, fabrication is relatively easy with chemical or lithographic methods so that ordered structures of metallic nanorods are potential candidates for a variety of applications. Taking advantage of their strongly anisotropic optical properties one can design polarization filters²⁹ while under certain conditions anisotropy results in negative refraction.^{30,31} Tapered nanorod arrays are also considered for hyperlensing since plasmons can travel through coupled metallic nanoparticles transferring near field energy along the nanorods to relatively long distances and then couple to conventional optics to generate the image.³² In the same context, nanorod chains were proposed to achieve both long propagation length and broadband operation toward color subwavelength imaging.³³ Metallic nanorod arrays cause large enhancement of the EM field and are considered for surface enhanced Raman scattering.³⁴ Moreover, they are more sensitive to changes in the dielectric constant of the environment compared to isolated nanorods.²² When the nanorods approach each other, the EM

field is concentrated in the interstitial region^{35–38} and longitudinal standing waves are formed in the dielectric space between the rods,²² similarly to plasmonic cavity resonators. Periodic assemblies of metallic nanorods also exhibit an interesting optical response when the diffraction condition resonates with the plasmon excitation frequency and new energy channels open up, giving rise to narrow resonances.^{39,40}

Though various aspects of the optical response of periodic structures of metallic nanorods have been extensively discussed in the literature, a systematic study with a rigorous analysis of the different collective plasmons and the other resonant optical modes of these systems is still missing. In this paper we report a thorough theoretical study of the optical response of ordered assemblies of metallic nanorods, of circular cross section, through accurate full-electrodynamic calculations using an extended version of the layer-multiple-scattering method,^{41–43} which enables physical insight. We consider hexagonal arrays of silver nanorods, aligned parallel to their axis. Such structures can be easily fabricated using porous alumina templates which are filled with a metal. We first analyze single metallic nanorods and present a consistent classification of their plasmon modes based on group theoretical arguments and diagonalization of the corresponding scattering matrix. Next, we focus on two-dimensional (2D) periodic arrays of silver nanorods, with diameter 20 nm and varying aspect ratio and lattice constant. We report a systematic study of their optical properties and explain effects resulting from interparticle interaction. We reveal the existence of collective plasmonic modes confined within the slab and provide a consistent interpretation of all bound and quasibound modes of the system. Finally, we consider three-dimensional (3D) crystals of metallic nanorods and investigate the complex band structure in conjunction with relevant extinction spectra of finite slabs of these crystals. Emphasis is placed on some peculiar features of their optical response, which arise from the existence of surface resonances that lead to interesting effects in the presence of a supporting substrate.

Our aim is the study of realistic systems of silver nanorods, described by the actual dielectric function of silver.⁴⁴ However, in some cases, a clear physical interpretation is easier if we use the Drude dielectric function⁴⁵

$$\epsilon_m(\omega) = 1 - \frac{\omega_p^2}{\omega(\omega + i\tau^{-1})}, \quad (1)$$

where ω_p is the bulk plasma frequency and τ is the relaxation time of the conduction-band electrons of the metal, which accounts for dissipative losses. When using the Drude dielectric function of Eq. (1), it is convenient to express the frequency in units of ω_p and consider c/ω_p as the length unit, where c is the velocity of light in vacuum. We note that, assuming a typical value of 10 eV for $\hbar\omega_p$, c/ω_p corresponds to about 20 nm.

II. PLASMON MODES OF SINGLE METALLIC NANORODS

The optical properties of single metallic nanorods have been studied by several authors.^{3–7} An important conclusion

is that it is essentially the length-to-diameter (L/D) aspect ratio which determines the resonance wavelengths and, by varying the aspect ratio, one can shift the dipolar plasmon resonances across the visible spectrum. The fundamental longitudinal resonance wavelength of an isolated metallic nanorod increases almost linearly with the particle aspect ratio. Interestingly, this resonance appears at wavelengths much longer than those of an ideal half-wave dipole antenna ($L = \lambda/2$). This is explained as follows. At optical frequencies the simple wavelength scaling $L = \lambda/2$ breaks down because incident radiation is no longer perfectly reflected from the metal's surface. Instead, the wave field penetrates into the metal and gives rise to surface-plasma oscillations. Hence, at optical frequencies an antenna does not respond to the external wavelength, λ , but to an effective wavelength, λ_{eff} , which depends on the material properties.⁴⁶ Most studies on single metallic nanorods focus on the dipolar resonance(s) while multipole resonances received considerably less attention.³ Here, we present a rigorous analysis of all plasmon modes of metallic nanorods based on group theory.

Let us assume the general case of a single particle characterized by a (relative) dielectric function ϵ_s and a (relative) magnetic permeability μ_s , centered at the origin of coordinates, in an otherwise homogeneous host medium of different dielectric function ϵ and magnetic permeability μ . An incident plane EM wave of angular frequency ω and wave vector \mathbf{q} has an electric field component $\mathbf{E}_0(\mathbf{r}, t) = \text{Re}[\mathbf{E}_0(\mathbf{r})\exp(-i\omega t)]$. $\mathbf{E}_0(\mathbf{r})$ can be expanded into regular vector spherical waves about the origin, as follows:⁴⁷

$$\mathbf{E}_0(\mathbf{r}) = \sum_{\ell=1}^{\infty} \sum_{m=-\ell}^{\ell} \left\{ a_{1\ell m}^0 j_{\ell}(qr) \mathbf{X}_{\ell m}(\hat{\mathbf{r}}) + \frac{i}{q} a_{2\ell m}^0 \nabla \times j_{\ell}(qr) \mathbf{X}_{\ell m}(\hat{\mathbf{r}}) \right\}, \quad (2)$$

where j_{ℓ} are the spherical Bessel functions which are finite everywhere; $\mathbf{X}_{\ell m}(\hat{\mathbf{r}})$ are the vector spherical harmonics; and $a_{P\ell m}^0$, $P=1, 2$, are appropriate coefficients of the magnetic and electric multipole fields, respectively. The total scattered wave, outside the scatterer, can be expanded in a similar manner

$$\mathbf{E}_{\text{sc}}(\mathbf{r}) = \sum_{\ell=1}^{\infty} \sum_{m=-\ell}^{\ell} \left\{ a_{1\ell m}^+ h_{\ell}^+(qr) \mathbf{X}_{\ell m}(\hat{\mathbf{r}}) + \frac{i}{q} a_{2\ell m}^+ \nabla \times h_{\ell}^+(qr) \mathbf{X}_{\ell m}(\hat{\mathbf{r}}) \right\}, \quad (3)$$

where h_{ℓ}^+ are the spherical Hankel functions appropriate for outgoing spherical waves: $h_{\ell}^+(qr) \approx (-i)^{\ell} \exp(iqr)/iqr$ as $r \rightarrow \infty$.

The scattering properties of the particle are determined through the so-called T matrix, which relates the amplitudes of the spherical-wave components of the scattered EM field to those of the incident field

$$a_{p\ell m}^+ = \sum_{p'\ell'm'} T_{p\ell m; p'\ell'm'} a_{p'\ell'm'}^0 \quad (4)$$

For the numerical evaluation of the elements of the T matrix for the nanorods that will be considered in the present work, we employ the extended-boundary-condition (EBC) method,⁴⁸ properly modified.⁴³ Truncating the relevant angular-momentum expansions at $\ell_{\max}=12$, $\ell_{\text{cut}}=16$, and using a Gaussian quadrature integration formula with 4000 points for the integrals involved is sufficient to obtain well-converged results.

The particle eigenmodes are obtained in the absence of incoming wave. In general, a single particle supports resonant modes of the EM field at the poles of the eigenvalues of the corresponding T matrix in the lower complex-frequency half plane near the real axis. For nonspherical scatterers, the T matrix is not diagonal in the spherical-wave basis and thus no unambiguous classification of its eigenvalues, according to polarization and angular momentum, can be made. Though the particle-plasmon modes usually have a predominant polarization and 2^ℓ -pole character,³ a rigorous assignment can be made by using group theory.⁴⁹ The different modes have the symmetry of the irreducible representations of the appropriate point group which, in the case of particles of cylindrical symmetry, is the $D_{\infty h}$ group.⁵⁰ A given mode can be excited only if the electric field component of the incident light has a nonvanishing projection into the appropriate irreducible subspace. For example, a plane EM wave incident at an angle θ ($0 < \theta < \pi/2$) with respect to the particle axis (taken as the z axis) can excite modes of $A_{1u}, A_{2g}, E_{|m|g}, E_{|m|u} \forall m$ symmetry if it is polarized normally to the particle axis (s polarization) and modes of $A_{1g}, A_{2u}, E_{|m|g}, E_{|m|u} \forall m$ symmetry if it is polarized in the plane of incidence defined by the direction of incidence and the particle axis (p polarization).

Figure 1 displays the scattering and absorption cross sections, normalized to the geometric cross section, for a single metallic nanorod in air. In the upper diagrams, the rod is described by the Drude dielectric function given by Eq. (1) without dissipative losses ($\tau^{-1}=0$), and has a diameter $D \equiv 2S=c/\omega_p$ and a length $L=2.5c/\omega_p$. In this case, obviously, the absorption cross section vanishes identically. An incoming p -polarized (left-hand diagram) or s -polarized (right-hand diagram) plane wave is incident at an angle $\theta=45^\circ$ with respect to the rod axis. The excitation of several particle-plasmon modes is clearly visible in the figure. Their eigenfrequencies, symmetry and predominant character are listed in Table I. In the lower diagrams of Fig. 1 we show the corresponding results for an actual silver nanorod, of dimensions $D=20$ nm and $L=50$ nm, in air. Here, for the dielectric function of silver we interpolate to the bulk values measured by Johnson and Christy⁴⁴ that include dissipative losses. It can be seen from the figure that, in the frequency region which interests us here, only the dipolelike resonances of short lifetime manifest themselves in the scattering and/or absorption cross sections. The particle-plasmon modes which have very long lifetimes compared to the absorption time are smoothed out by absorption.

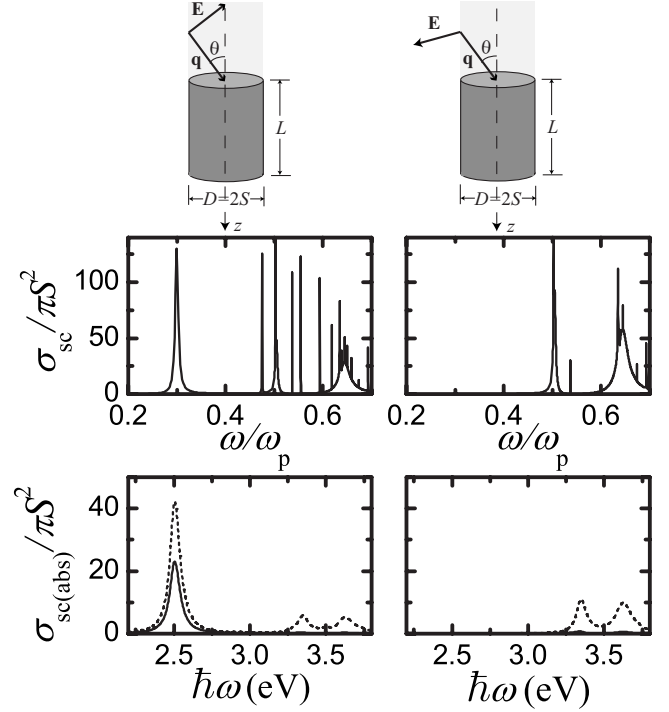


FIG. 1. The scattering (solid lines) and absorption (dashed lines) cross sections of a metallic nanorod in air, for p - (left-hand diagrams) and s - (right-hand diagrams) polarized light incident at an angle $\theta=45^\circ$ with respect to the rod axis, as shown in the margin. In the upper diagrams, the dielectric function of the nanorod, of diameter $D=2S=c/\omega_p$ and length $L=2.5c/\omega_p$, is given by Eq. (1) with $\tau^{-1}=0$, which implies that the absorption cross section is identically zero. In the lower diagrams, the experimental dielectric function of bulk silver (Ref. 44) is used for a rod of dimensions $D=20$ nm and $L=50$ nm.

III. THE EXTENDED LAYER-MULTIPLE-SCATTERING METHOD

The calculations for 2D and 3D periodic structures of metallic nanorods that will be reported in this work are based on the extended layer-multiple-scattering method, which has been presented in detail elsewhere.^{41–43} Here we restrict ourselves to a brief description of the main points of the method.

The structures that can be dealt with by this method may consist of successive, possibly different, layers of scatterers arranged with the same 2D periodicity. The properties of the individual scatterers enter only through the corresponding T matrix which, for homogeneous spherical particles, is given by the closed-form solutions of the Mie-scattering problem, while for scatterers of arbitrary shape it is calculated numerically by the EBC method.⁴⁸ At a first step, in-plane multiple scattering is evaluated in the spherical-wave basis using proper propagator functions. Subsequently, interlayer scattering is calculated in a plane-wave basis through appropriate reflection and transmission matrices. The scattering S matrix of a multilayer slab, which transforms the incident into the outgoing wave field, is obtained by combining the reflection and transmission matrices of the individual component layers in an appropriate manner. As noted here above, the scatterers, as well as the host material, may be different in the

TABLE I. Plasmon modes of a single metallic nanorod, described by the Drude dielectric function without dissipative losses, in air ($D=c/\omega_p$ and $L=2.5c/\omega_p$). The asterisk indicates the modes of relatively short lifetime, i.e., the broader resonances.

Eigenfrequency (in units of ω_p)	Symmetry	Predominant character
0.2989*	A_{2u}	Electric dipole
0.4747	A_{1g}	Electric quadrupole
0.5024	E_{1g}	Electric quadrupole/16-pole
0.5044*	E_{1u}	Electric dipole
0.5377	E_{2g}	Electric quadrupole
0.5546	A_{2u}	Electric dipole
0.5936	A_{1g}	Electric quadrupole
0.6187	A_{2u}	Electric dipole
0.6345	E_{1g}	Electric quadrupole/16-pole
0.6377	A_{1g}	Electric quadrupole
0.6385	E_{1u}	Electric dipole/octapole/32-pole
0.6439*	E_{1u}	Electric dipole
0.6449	E_{1g}	Electric quadrupole/16-pole
0.6501	A_{2u}	Electric dipole
0.6585	A_{1g}	Electric quadrupole
0.6737	E_{2g}	Electric quadrupole
0.6927	E_{2g}	Electric quadrupole

different layers; the scatterers need only have the same 2D periodicity. As a special case, a layer can be a homogeneous plate or a planar interface between two different homogeneous media. The reflection and transmission matrices are then obtained directly by Fresnel equations⁴⁷ but this possibility allows one to describe composite structures which are used in an actual experiment and include, e.g., a homogeneous spacer layer and/or a supporting substrate.^{49,51} The ratio of the transmitted or reflected energy flux associated with the incident wave defines the transmittance, \mathcal{T} , or reflectance, \mathcal{R} , of the slab, respectively.

On the other hand, for a 3D crystal consisting of an infinite periodic sequence of layers, stacked along the z direction, applying the Bloch condition for the wave field in the region between two consecutive unit slabs leads to an eigenvalue equation, which gives the z component of the Bloch wave vector, k_z , for given frequency ω and in-plane reduced wave-vector component \mathbf{k}_\parallel , which are conserved quantities in the scattering process. The eigenvalues $k_z(\omega, \mathbf{k}_\parallel)$, looked upon as functions of real ω , define, for each \mathbf{k}_\parallel , lines (sometimes they are called real-frequency lines) in the complex k_z plane. Taken together they constitute the complex band structure of the infinite crystal associated with the given crystallographic plane. A line of given \mathbf{k}_\parallel may be real (in the sense that k_z is real) over certain frequency regions and be complex (in the sense that k_z is complex) for ω outside these regions. It turns out that for given \mathbf{k}_\parallel and ω , out of the eigenvalues $k_z(\omega, \mathbf{k}_\parallel)$ none or, at best, a few are real and the corresponding eigenvectors represent propagating modes of the EM field in the given infinite crystal. The remaining eigenvalues $k_z(\omega, \mathbf{k}_\parallel)$ are complex and the corresponding eigenvectors

represent evanescent waves. These have an amplitude which increases exponentially in the positive or negative z direction and, unlike the propagating waves, do not exist as physical entities in the infinite crystal. However, they are an essential part of the physical solutions of the EM field in a slab of finite thickness. A region of frequency where propagating waves do not exist, for given \mathbf{k}_\parallel , constitutes a frequency gap of the EM field for the given \mathbf{k}_\parallel . If over a frequency region no propagating wave exists whatever the value of \mathbf{k}_\parallel , then this region constitutes an absolute frequency gap.

In order to ensure adequate convergence in our calculations for the structures that will be considered in the present work, we truncate the spherical-wave expansions at $\ell_{\max}=12$ and take into account 151 2D reciprocal lattice vectors in the relevant plane-wave expansions while the single-particle scattering T matrix is evaluated with $\ell_{\text{cut}}=16$ and a Gaussian quadrature integration formula with 4000 points.

IV. ARRAYS OF ALIGNED METALLIC NANORODS

Before embarking into the discussion of the optical response of ordered arrays of metallic nanorods, we present some convergence tests of the extended layer-multiple-scattering method. The EBC technique, which is employed for the evaluation of the single-particle scattering T matrix, is based on spherical-wave expansions of the EM field and convergence problems are expected for scatterers with strong deviation from the spherical shape, like the nanorods we consider here. We note that metallic particles encounter more severe convergence problems compared to dielectric particles due to the large refractive index contrast between metal and dielectric environment.⁴⁸ Moreover, the study of multiple scattering in a periodic array puts more stringent accuracy requirements on the calculation of the T matrix, compared to usual average cross-section calculations for randomly oriented isolated nanoparticles.

As an example of the accuracy expected from multiple-scattering calculations with the extended MULTTEM code,⁴¹⁻⁴³ we show in Fig. 2 the extinction spectrum (extinction = negative logarithm of the transmittance) of a free-standing hexagonal array of silver nanorods, aligned parallel to their axis, for p -polarized light incident at an angle $\theta=45^\circ$, calculated with three different realizations of the system. The rods have a diameter $D=20$ nm and a length $L=50$ nm while the lattice constant is chosen $a=100$ nm to minimize the interaction between the nanorods. For the permittivity of silver we interpolate to the bulk values measured by Johnson and Christy.⁴⁴ In the first realization we consider a single plane of nanorods with $D=20$ nm and $L=50$ nm. In the second realization, the system is built of two identical consecutive planes of touching nanorods with $D=20$ nm and $L=25$ nm. This calculation, obviously, involves, in addition, interplanar multiple scattering. Finally, we consider a third realization of the system by slicing the rods in three unequal parts of lengths 20, 20, and 10 nm. This calculation involves all multiple-scattering events between the three consecutive planes of touching nanorods. All other parameters were kept the same in the three calculations. The comparison between the different spectra in Fig. 2 shows that all features of the

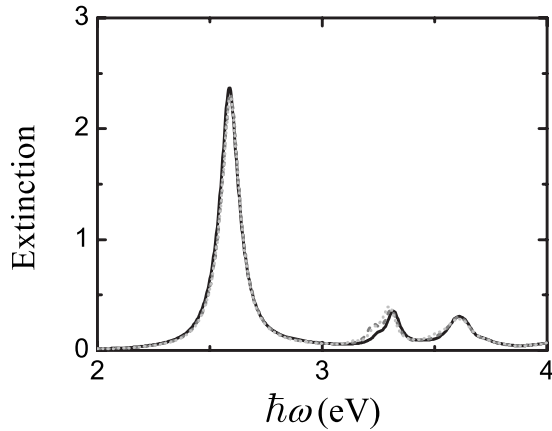


FIG. 2. Extinction spectrum of a free-standing hexagonal array ($a=100$ nm) of aligned silver nanorods ($D=20$ nm and $L=50$ nm), for p -polarized light incident at an angle $\theta=45^\circ$, calculated with three different realizations of the system: one plane of nanorods with $D=20$ nm and $L=50$ nm (full line). Two identical consecutive planes of touching nanorods with $D=20$ nm and $L=25$ nm (dashed line). Three consecutive planes of touching nanorods with $D=20$ nm and $L=20, 20$, and 10 nm (dotted line).

extinction spectrum are well reproduced by the different calculations.

We now consider free-standing hexagonal arrays of aligned silver nanorods of fixed diameter $D=20$ nm and varying length and lattice constant. Figure 3 depicts extinction spectra of such monolayers of rods with $L=50, 100$, and 150 nm, illuminated by p -polarized light incident at an angle $\theta=45^\circ$, as a function of the lattice constant a . Interaction between plasmons of the individual particles gives rise to corresponding collective plasmon modes, which manifest themselves as peaks in the extinction spectra of these arrays. We note that, under illumination at normal incidence or at an angle with s -polarized light, the longitudinal modes are not efficiently excited since, in these cases, the electric field of the incident EM wave oscillates perpendicularly to the particle axis and no extinction peak appears at the corresponding frequencies. At oblique incidence, a p -polarized incident wave excites both longitudinal and transverse collective plasmon modes, as can be seen in Fig. 3. The fundamental dipole

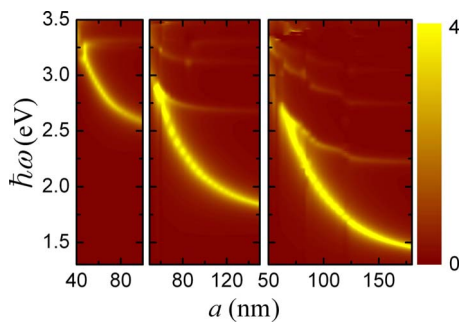


FIG. 3. (Color online) Extinction spectra for p -polarized light incident at an angle $\theta=45^\circ$ on hexagonal arrays (lattice constant a) of aligned silver nanorods with diameter $D=20$ nm and length $L=50$ nm (left-hand diagram), $L=100$ nm (middle diagram) and $L=150$ nm (right-hand diagram).

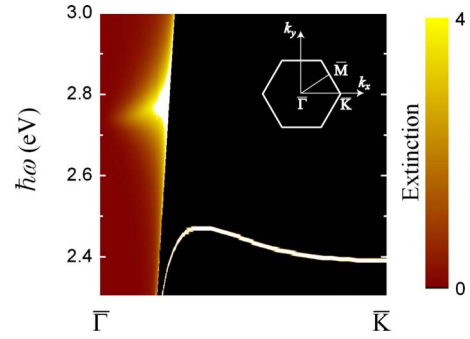


FIG. 4. (Color online) Extinction spectra of a free-standing hexagonal array ($a=70$ nm) of aligned silver nanorods ($L=50$ nm and $D=20$ nm) about the eigenfrequency of their fundamental plasmon mode, for light incident with \mathbf{k}_\parallel along the $\bar{\Gamma}\bar{K}$ direction of the surface Brillouin zone shown in the inset. In the dark region, outside the light cone, the white curve shows the dispersion of the corresponding collective eigenmodes of the array.

longitudinal mode gives the most pronounced extinction peak, which varies strongly with the aspect ratio and lattice constant. Dipole transverse modes and higher-order modes manifest themselves as smaller peaks at higher frequencies. To understand the different spectral features, we first concentrate on the larger lattice constants for the different particle lengths considered, i.e., the rightmost parts of the three diagrams of Fig. 3. In this case, the optical response is close to that of isolated nanorods discussed in the previous section and the dipole longitudinal resonance rapidly shifts to lower frequencies with increasing particle length. As the lattice constant decreases and the nanorods approach each other, interparticle coupling leads to a strong blueshift of the low-frequency longitudinal resonance while the position of the high-frequency resonances is much less affected. At small lattice constants, longitudinal and transverse resonances overlap in frequency and no clear character can be assigned to the collective plasmon excitation. It is interesting that the spectral position of the fundamental dipole longitudinal plasmon mode can be tuned within a broad range extending from infrared to ultraviolet frequencies by changing the lattice constant and the nanorod aspect ratio with the longer particles exhibiting stronger tunability. Generally, longer rods show a richer spectrum with a larger number of plasmon modes. Our results are in line with recent experimental and theoretical studies on arrays of longer gold nanorods, fabricated by electrodeposition into thin nanoporous anodized aluminum oxide templates.^{38,29}

In Fig. 4 we show the extinction spectra of one of the above monolayers of nanorods (that for $a=70$ nm, $D=20$ nm, and $L=50$ nm) about the eigenfrequency of the fundamental plasmon mode, for light incident with $\mathbf{k}_\parallel=(k_x, 0)$, $0 \leq k_x \leq 4\pi/3a$, i.e., along the $\bar{\Gamma}\bar{K}$ direction of the surface Brillouin zone shown in the inset of Fig. 4. By increasing k_x , the component of the electric field of the p -polarized incident wave along the rods becomes larger and thus the longitudinal plasmon modes are excited more efficiently leading to stronger resonance peaks in the extinction spectrum. In the dark region of Fig. 4, outside the light cone, the white curve shows the dispersion of the corresponding

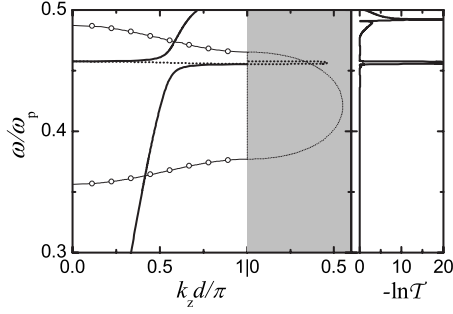


FIG. 5. A simple hexagonal crystal of free-standing metallic nanorods, described by the Drude dielectric function without dissipative losses, aligned parallel to their axis which is taken along the z direction. Rod diameter: $D=c/\omega_p$. Rod length: $L=2.5c/\omega_p$. Lattice constants: $a=3c/\omega_p$ and $d=3c/\omega_p$. Left-hand diagram: the complex photonic band structure along the $[001]$ direction. The complex bands are displayed with dotted lines with the imaginary part of k_z plotted in the shaded area. The thick and thin lines show the doubly degenerate and nondegenerate bands, respectively. Right-hand diagram: extinction of light incident normally of a slab of eight (001) planes of the above crystal.

collective eigenmodes of the array. These are plasmonic modes confined within the layer of rods and cannot be excited by an externally incident wave. Outside the layer they have the form of evanescent waves and cannot match continuously a propagating mode of the EM field; photon momentum and energy cannot be conserved simultaneously. The frequency dispersion of these bound modes, which are important for subwavelength imaging,^{32,33} can be tuned within the range of infrared and visible frequencies by changing the materials and geometric parameters of the structure. In particular, we note the existence of a flat region in the dispersion curve within a very narrow frequency window, $2.465 \text{ eV} < \hbar\omega < 2.475 \text{ eV}$, and a rather large interval of propagation constants, $0.4\pi < k_{\parallel}a < 0.6\pi$. These exotic zero (and nearly zero) group-velocity modes, and their role in evanescent-wave enhancement and subwavelength imaging, have also been discussed by others, e.g., in chains of silver spheres.⁵²

V. THREE-DIMENSIONAL CRYSTALS OF METALLIC NANORODS

We now consider an infinite 3D crystal built of consecutive layers, parallel to the xy plane, of identical, free-standing metallic nanorods aligned parallel to their axis (z direction). We assume that the metallic material is described by the Drude dielectric function of Eq. (1) without dissipative losses ($\tau^{-1}=0$), in order to ensure an unambiguous interpretation of the photonic band structure of the given crystal. The nanorods, of diameter $D=c/\omega_p$ and length $L=2.5c/\omega_p$, in each layer are arranged on a hexagonal lattice with lattice constant $a=3c/\omega_p$, while adjacent planes of nanorods are displaced by the vector $(0,0,d)$, where $d=3c/\omega_p$.

The left-hand diagram of Fig. 5 shows the complex photonic band structure of the crystal under consideration along the $[001]$ direction, i.e., for $\mathbf{k}_{\parallel}=\mathbf{0}$. The symmetry of the

bands along this direction is that of the C_{6v} group.⁵⁰ At low frequencies we obtain a linear dispersion curve, of E_1 symmetry (doubly degenerate), as expected for propagation in a homogeneous effective medium characterized by a frequency-independent refractive index. In addition to this extended band, flat bands are formed from the particle-plasmon modes of the individual nanorods that interact weakly between them. Along the $[001]$ direction, in the frequency region under consideration, there is one doubly degenerate flat band, also of E_1 symmetry, which originates from the E_{1g} particle-plasmon modes (see Fig. 1 and Table I). This band hybridizes with the extended band that would be in the effective medium, leading to a narrow gap about $0.46\omega_p$. Moreover, there are two nondegenerate A_1 flat bands, about $0.36\omega_p$ and $0.47\omega_p$, which originate from the low-lying A_{2u} and A_{1g} particle-plasmon modes, respectively. These nondegenerate bands do not interact with the effective-medium band because they have not the same symmetry and, also, they cannot be excited by an externally incident wave. They arise from an apparently weak interaction between corresponding bound states of the EM field, localized about consecutive (001) layers of the given crystal. Indeed, the eigenfrequencies of a slab of $N_L=8$ such planes of nanorods, for $\mathbf{k}_{\parallel}=\mathbf{0}$, plotted against values of the reduced wavenumber $k_z=\kappa\pi/(N_L+1)c$, $\kappa=1,2,\dots,N_L$, with $N_L=8$, reproduce the corresponding dispersion curves of the infinite crystal, as shown by the open circles in the left-hand diagram of Fig. 5.

Apart from the ordinary frequency bands (real k_z), the left-hand diagram of Fig. 5 also displays real-frequency lines for complex eigenvalues k_z . These lines are the analytic continuations of the ordinary bands in the complex k_z plane.⁵³ The real-frequency line of the appropriate symmetry (E_1 in the present case) with the smallest in magnitude imaginary part of k_z over a frequency gap determines the attenuation of the wave field over this region. The extinction of a finite slab of the crystal, consisting of N_L (001) planes, is

$$-\ln \mathcal{T}(\omega) = 2dN_L |\text{Im}[k_z(\omega)]| + \text{constant} \quad (5)$$

for a given value of \mathbf{k}_{\parallel} . This is indeed observed in the right-hand diagram of Fig. 5, which depicts the extinction of a slab of the crystal under consideration, consisting of $N_L=8$ (001) planes of nanorods, at normal incidence. It is worth noting that, apart from the strong extinction in the gap region about $0.46\omega_p$, there is a second sharp extinction peak about $0.49\omega_p$, i.e., within the region of a band where propagating modes do exist in the infinite crystal. Interestingly, this second peak remains practically the same by changing the size of the slab, in contrast with Eq. (5) which predicts a linear increase in the extinction with the size of the slab in gap regions, and should be ascribed to a surface resonance. It is also interesting that a higher resolution reveals that this peak is double, as expected for two weakly interacting resonances, one at each surface of the slab.

The left-hand panel of Fig. 6 displays the complex photonic band structure of the given crystal for $\mathbf{k}_{\parallel}=(0,2\pi/a,0)$. For $\mathbf{k}_{\parallel}=(k_x,0)$, $0 < k_x < 4\pi/3a$, i.e., along the $\bar{\Gamma}\bar{K}$ direction of the surface Brillouin zone, the point group of the wave

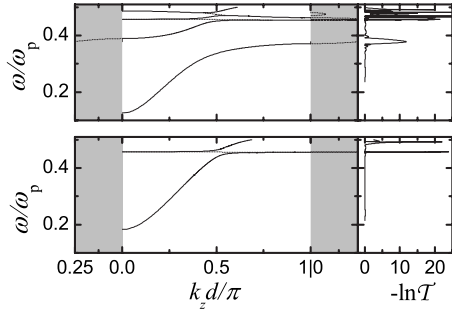


FIG. 6. Left-hand panel: complex photonic bands of Q_1 (upper diagram) and Q_2 (lower diagram) symmetry of the crystal of Fig. 5, for $\mathbf{k}_{\parallel}=(0.2\pi/a,0)$. Right-hand panel: extinction of p - (upper diagram) and s - (lower diagram) polarized light incident on a slab of eight (001) planes of the given crystal with $\mathbf{q}_{\parallel}=(0.2\pi/a,0)$.

vector is the C_{1h} group and the electric field eigenmodes can be classified as even (Q_1) or odd (Q_2) upon reflection with respect to the xz plane. According to group theory, a doubly degenerate band of E_1 symmetry (for $\mathbf{k}_{\parallel}=\mathbf{0}$) splits for $\mathbf{k}_{\parallel}=(k_x,0)$ into one band of Q_1 and one of Q_2 symmetry; similarly, an A_1 band gives a Q_1 band, as shown in the left-hand panel of Fig. 6. A p - or s -polarized EM wave incident on a finite (001) slab of the crystal with $\mathbf{k}_{\parallel}=(k_x,0)$ excites bands of Q_1 or Q_2 symmetry, respectively, and through them is transmitted to the other side of the slab. In the regions of frequency gaps, where there are no propagating Bloch modes, the transmission coefficient is determined from the complex band of the proper symmetry which has the smallest imaginary part: the wave decreases exponentially within the slab with an attenuation coefficient equal to $|\text{Im } k_z(\omega)|$ of this band, as shown in the right-hand panel of Fig. 6.

VI. EFFECT OF A SUBSTRATE

So far, we investigated free-standing periodic arrays of silver nanorods, aligned parallel to their axis. As a typical example, in Fig. 7 we show by solid lines the extinction spectrum of such a hexagonal array with $D=20$ nm, $L=50$ nm, and $a=70$ nm, for light incident at an angle $\theta=45^\circ$. As discussed in Sec. IV, the spectrum associated with an s -polarized incident wave is characterized by resonance peaks at relatively high frequencies, which correspond to the excitation of dipole transverse and higher-order collective plasmon modes. For a p -polarized incident wave we obtain, in addition, a strong low-frequency resonance, which corresponds to the excitation of the fundamental dipole longitudinal collective plasmon mode. If the given array of rods is standing on a supporting substrate, an additional resonance peak appears in the frequency region of interest, for both polarization modes, and this peak shifts down to lower frequencies with increasing dielectric constant of the substrate. For a silica substrate ($\epsilon_{\text{silica}}=2.13$), this peak is situated at 3.07 eV and the fundamental longitudinal resonance is slightly shifted to lower frequencies, while for an indium tin oxide substrate ($\epsilon_{\text{ITO}}=3.6$) this peak shifts down to 2.75 eV and appears as a shoulder of the fundamental longitudinal resonance peak. As we showed by systematic numerical cal-

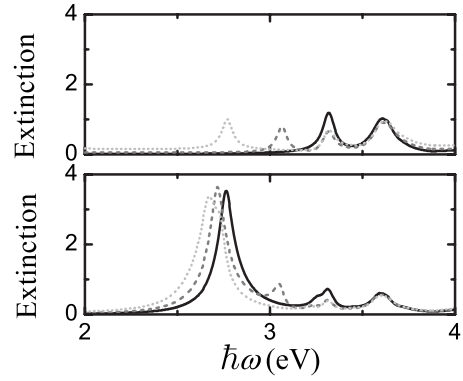


FIG. 7. Extinction of s - (upper diagram) and p - (lower diagram) polarized light, incident at an angle $\theta=45^\circ$ on a monolayer of silver nanorods on different substrates. The nanorods have dimensions $D=20$ nm and $L=50$ nm, and are arranged on a hexagonal lattice of lattice constant $a=70$ nm with their axis perpendicular to the substrate. Solid lines: free-standing nanorods (without substrate). Dashed lines: nanorods standing on a semi-infinite silica substrate (dielectric constant: $\epsilon_{\text{silica}}=2.13$). Dotted line: nanorods standing on a semi-infinite indium tin oxide substrate ($\epsilon_{\text{ITO}}=3.6$).

culations, this additional peak is due to the surface resonance discussed in Sec. V: at an interface between the monolayer of nanorods and a low-permittivity dielectric medium, such as air, this mode is at relatively high frequencies, outside the considered frequency range. By increasing the dielectric constant of the substrate, this interface resonance is redshifted and appears at visible frequencies, interacting with the other modes of the system, as shown in Fig. 7.

VII. CONCLUSION

In summary, we reported a systematic study of the optical response of single- and multilayer architectures of ordered assemblies of metallic nanorods, aligned parallel to their axis, by means of full-electrodynamic calculations using the extended layer-multiple-scattering method and showed that the method retains its high efficiency and accuracy even in cases of particles with edges and strong deviation from the spherical shape. We first presented a rigorous analysis of the plasmon modes of single metallic nanorods of circular cross section and their coupling to an externally incident wave, based on group theory. Next, we investigated 2D hexagonal arrays of aligned silver nanorods with varying aspect ratio and lattice constant. We analyzed the formation of collective plasmon modes of different character and provided a consistent interpretation of the underlying physics. More specifically, we showed that such longitudinal modes exhibit polarization selectivity and tunability in the range of visible and infrared frequencies, properties which are very useful for filtering and sensing applications. Outside the light cone, these modes are confined within the slab and also exhibit strong tunability. Of particular interest is the existence of a flat region in the dispersion relation of these modes within a narrow frequency window and a large interval of propagation constants. This makes metallic nanorod arrays useful for evanescent-wave-enhancement and subwavelength-imaging

applications. Finally, we investigated 3D crystals of metallic nanorods and analyzed the complex band structure in conjunction with relevant extinction spectra of finite slabs of these crystals. In particular, we explained some peculiar spectral features which are due to the existence of surface resonances and can modify the optical response of the sys-

tem in a controllable manner by using a supporting substrate.

ACKNOWLEDGMENTS

This work was supported by the research program “Kapodistrias” of the University of Athens.

- ¹S. A. Maier, *Plasmonics: Fundamentals and Applications* (Springer, Dordrecht, 2007); *Surface Plasmon Nanophotonics*, Springer Series in Optical Sciences, Vol. 131, edited by M. L. Brongersma and P. G. Kik, (Springer, Dordrecht, 2007); *Nanophotonics with Surface Plasmons*, Advances in Nano-optics and Nano-photonics, edited by V. M. Shalaev and S. Kawata (Elsevier, Oxford, 2007).
- ²K.-S. Lee and M. A. El-Sayed, *J. Phys. Chem. B* **109**, 20331 (2005).
- ³B. N. Khlebtsov and N. G. Khlebtsov, *J. Phys. Chem. C* **111**, 11516 (2007).
- ⁴K. Imura, T. Nagahara, and H. Okamoto, *J. Chem. Phys.* **122**, 154701 (2005).
- ⁵A. Brioude, X. C. Jiang, and M. P. Pileni, *J. Phys. Chem. B* **109**, 13138 (2005).
- ⁶S. W. Prescott and P. Mulvaney, *J. Appl. Phys.* **99**, 123504 (2006).
- ⁷M. Liu, P. Guyot-Sionnest, T.-W. Lee, and S. K. Gray, *Phys. Rev. B* **76**, 235428 (2007).
- ⁸C. L. Nehl and J. H. Hafner, *J. Mater. Chem.* **18**, 2415 (2008).
- ⁹S. J. Oldenburg, R. D. Averitt, S. L. Westcott, and N. J. Halas, *Chem. Phys. Lett.* **288**, 243 (1998).
- ¹⁰J. Chen, B. Wiley, Z.-Y. Li, D. Campbell, F. Saeki, H. Cang, L. Au, J. Lee, X. Li, and Y. Xia, *Adv. Mater.* **17**, 2255 (2005).
- ¹¹A. Sánchez-Iglesias, I. Pastoriza-Santos, J. Pérez-Juste, B. Rodríguez-González, F. J. García de Abajo, and L. M. Liz-Marzán, *Adv. Mater.* **18**, 2529 (2006).
- ¹²M. Liu and P. Guyot-Sionnest, *J. Phys. Chem. B* **109**, 22192 (2005).
- ¹³E. Prodan, C. Radloff, N. J. Hallas, and P. Nordlander, *Science* **302**, 419 (2003).
- ¹⁴P. K. Jain, S. Eustis, and M. A. El-Sayed, *J. Phys. Chem. B* **110**, 18243 (2006).
- ¹⁵B. Willingham, D. W. Brandl, and P. Nordlander, *Appl. Phys. B: Lasers Opt.* **93**, 209 (2008).
- ¹⁶Y. A. Urzhumov, G. Shvets, J. Fan, F. Capasso, D. Brandl, and P. Nordlander, *Opt. Express* **15**, 14129 (2007).
- ¹⁷M. Moskovits, *Rev. Mod. Phys.* **57**, 783 (1985).
- ¹⁸J.-H. Song, T. Atay, S. Shi, H. Urabe, and A. V. Nurmikko, *Nano Lett.* **5**, 1557 (2005).
- ¹⁹E. Fort and S. Grésillon, *J. Phys. D* **41**, 013001 (2008).
- ²⁰R. M. Bakker, V. P. Drachev, Z. Liu, H.-K. Yuan, R. H. Pedersen, A. Boltasseva, J. Chen, J. Irudayaraj, A. V. Kildishev, and V. M. Shalaev, *New J. Phys.* **10**, 125022 (2008).
- ²¹C. J. Murphy, A. M. Gole, S. E. Hunyadi, J. W. Stone, P. N. Sisco, A. Alkilany, B. E. Kinard, and P. Hankins, *Chem. Commun. (Cambridge)* **2008**, 544 (2008).
- ²²D. P. Lyvers, J.-M. Moon, A. V. Kildishev, V. M. Shalaev, and A. Wei, *ACS Nano* **2**, 2569 (2008).
- ²³S. A. Maier, P. G. Kik, and H. A. Atwater, *Appl. Phys. Lett.* **81**, 1714 (2002).
- ²⁴E. Ozbay, *Science* **311**, 189 (2006).
- ²⁵G. Gantzounis and N. Stefanou, *Phys. Rev. B* **74**, 085102 (2006).
- ²⁶Z. Yu, G. Veronis, Z. Wang, and S. Fan, *Phys. Rev. Lett.* **100**, 023902 (2008).
- ²⁷T. W. Ebbesen, C. Genet, and S. I. Bozhevolnyi, *Phys. Today* **61**, 44 (2008).
- ²⁸K. R. Catchpole and A. Polman, *Appl. Phys. Lett.* **93**, 191113 (2008).
- ²⁹R. Kulloock, W. R. Hendren, A. Hille, S. Grafström, P. R. Evans, R. J. Pollard, R. Atkinson, and L. M. Eng, *Opt. Express* **16**, 21671 (2008).
- ³⁰W. T. Lu and S. Sridhar, *Phys. Rev. B* **77**, 233101 (2008).
- ³¹Y. Liu, G. Bartal, and X. Zhang, *Opt. Express* **16**, 15439 (2008).
- ³²A. Ono, J.-I. Kato, and S. Kawata, *Phys. Rev. Lett.* **95**, 267407 (2005).
- ³³S. Kawata, A. Ono, and P. Verma, *Nat. Photonics* **2**, 438 (2008).
- ³⁴Y. Liu, J. Fan, Y.-P. Zhao, S. Shanmukh, and R. A. Dluhy, *Appl. Phys. Lett.* **89**, 173134 (2006).
- ³⁵R. Atkinson, W. R. Hendren, G. A. Wurtz, W. Dickson, A. V. Zayats, P. Evans, and R. J. Pollard, *Phys. Rev. B* **73**, 235402 (2006).
- ³⁶W. Dickson, G. A. Wurtz, P. Evans, D. O’Connor, R. Atkinson, R. Pollard, and A. V. Zayats, *Phys. Rev. B* **76**, 115411 (2007).
- ³⁷W. Dickson, P. Evans, G. A. Wurtz, W. Hendren, R. Atkinson, R. Pollard, and A. V. Zayats, *J. Microsc.* **229**, 415 (2008).
- ³⁸G. A. Wurtz, W. Dickson, D. O’Connor, R. Atkinson, W. Hendren, P. Evans, R. Pollard, and A. V. Zayats, *Opt. Express* **16**, 7460 (2008).
- ³⁹B. Auguie and W. L. Barnes, *Phys. Rev. Lett.* **101**, 143902 (2008).
- ⁴⁰V. G. Kravets, F. Schedin, and A. N. Grigorenko, *Phys. Rev. Lett.* **101**, 087403 (2008).
- ⁴¹N. Stefanou, V. Yannopapas, and A. Modinos, *Comput. Phys. Commun.* **113**, 49 (1998).
- ⁴²N. Stefanou, V. Yannopapas, and A. Modinos, *Comput. Phys. Commun.* **132**, 189 (2000).
- ⁴³G. Gantzounis and N. Stefanou, *Phys. Rev. B* **73**, 035115 (2006).
- ⁴⁴P. B. Johnson and R. W. Christy, *Phys. Rev. B* **6**, 4370 (1972).
- ⁴⁵N. W. Ashcroft and N. D. Mermin, *Solid State Physics* (Saunders, New York, 1976).
- ⁴⁶L. Novotny, *Phys. Rev. Lett.* **98**, 266802 (2007).
- ⁴⁷J. D. Jackson, *Classical Electrodynamics* (Wiley, New York, 1999).
- ⁴⁸M. I. Mishchenko, L. D. Travis, and A. A. Lacis, *Scattering, Absorption, and Emission of Light by Small Particles* (Cam-

bridge University Press, Cambridge, 2002).

⁴⁹G. Gantzounis, N. Stefanou, and N. Papanikolaou, Phys. Rev. B **77**, 035101 (2008).

⁵⁰J. F. Cornwell, *Group Theory in Physics* (Academic, London, 1984), Vol. 1.

⁵¹N. Stefanou and A. Modinos, J. Phys.: Condens. Matter **3**, 8135

(1991).

⁵²C. R. Simovski, A. J. Viitanen, and S. A. Tretyakov, Phys. Rev. E **72**, 066606 (2005).

⁵³G. Gantzounis and N. Stefanou, Phys. Rev. B **72**, 075107 (2005).